Top-down morphogenesis of colorectal tumors

Ie-Ming Shih*, Tian-Li Wang*, Giovanni Traverso*, Kathy Romans*, Stanley R. Hamilton†, Shmuel Ben-Sasson‡, Kenneth W. Kinzler*, and Bert Vogelstein*§

*The Howard Hughes Medical Institute, Johns Hopkins Oncology Center, and the Department of Pathology, Johns Hopkins Medical Institutions, Baltimore, MD 21231; †Division of Pathology and Laboratory Medicine, University of Texas M. D. Anderson Cancer Center, Houston, TX 77030; and ‡Department of Experimental Medicine and Cancer Research, Hebrew University-Hadassah Medical School, Jerusalem 91120, Israel

Contributed by Bert Vogelstein, December 28, 2000

One of the fundamental tenets of oncology is that tumors arise from stem cells. In the colon, stem cells are thought to reside at the base of crypts. In the early stages of tumorigenesis, however, dysplastic cells are routinely found at the luminal surface of the crypts whereas the cells at the bases of these same crypts appear morphologically normal. To understand this discrepancy, we evaluated the molecular characteristics of cells isolated from the bases and orifices of the same crypts in small colorectal adenomas. We found that the dysplastic cells at the tops of the crypts often exhibited genetic alterations of adenomatous polyposis coli (*APC*) and neoplasia-associated patterns of gene expression. In contrast, cells located at the base of these same crypts did not contain such alterations and were not clonally related to the contiguous transformed cells above them. These results imply that development of adenomatous polyps proceeds through a top-down mechanism. Genetically altered cells in the superficial portions of the mucosae spread laterally and downward to form new crypts that first connect to preexisting normal crypts and eventually replace them.

It is widely believed that cancer cells are derived from normal stem cells. Only such stem cells have an innate capacity for long-term proliferation and the ability to differentiate along several directions, features that characterize cancer (1). In the large intestine, detailed morphologic, biochemical, and physiologic studies have clearly shown that stem cells exist near the base of the crypts, a few cells away from the bottom of crypts (2). The progeny of stem cells migrate up the crypt, continuing to divide until they reach its mid-portion. Subsequently, the migrating epithelial cells stop dividing and instead differentiate to mature cells (largely mucous-secreting goblet cells and absorptive epithelial cells). When the differentiating cells reach the top of the crypt, they undergo apoptosis and are engulfed by stromal cells or shed into the lumen.

In light of this developmental architecture, it would be predicted that the neoplastic cells within early neoplasms should be derived from cells at the bases of the crypts and that such cells should give rise to new, completely dysplastic crypts that branch as the lesions expand. Histopathological examinations, however, have long shown that this expected pattern is not observed (3–7). As shown in Fig. 1, most early neoplastic lesions of the colon contain dysplastic cells only at the orifices and luminal surface of the crypts. One can easily follow continuous columns of epithelial cells within these crypts and observe that the epithelial cells abruptly change from dysplastic to normal midway down the crypt axis (Fig. 1*B*). By using radioactive thymidine and other markers of proliferation, it has been shown that the dysplastic cells at the orifices of the crypts have patterns expected of neoplastic cells whereas the cells at the base have normal proliferative patterns (4, 5, 8).

These marked distinctions between observation and expectation have stimulated investigators to propose several different models for the morphological development of adenomas. It has been suggested, e.g., that the stem cells that give rise to neoplasms are actually in the intercryptal zones that lie between crypt orifices rather than at the base of the crypts (3). Alternatively, it is possible that the normal-appearing epithelial cells at the base of small adenomatous crypts are actually transformed, and that the dysplastic appearance is only manifest as cells begin to differentiate and migrate up the crypt column (5, 9).

To distinguish between the various models and better understand the early stages of neoplasia, we sought to characterize the relevant cell populations at the molecular level. Our results conclusively demonstrate that the dysplastic cells in the upper parts of the crypts represent mutant clones that are genetically unrelated to the cells at the bottom of the crypt. These results exclude some models that have previously been considered, and implicate a top-down model for adenoma morphogenesis.

Materials and Methods

Tissues and Tumor DNA Samples. Formalin-fixed, paraffin-embedded tissue samples including 35 small sporadic adenomas (average diameter 2 mm, range 1–3 mm) were retrieved from the surgical pathology archives of Johns Hopkins Hospital. Lesions from patients with familial adenomatous polyposis or hereditary nonpolyposis colorectal cancer were excluded. Histologically, all adenomas demonstrated low-grade dysplasia without any foci of high-grade dysplasia or carcinoma. Ten small adenomatous polyps were selected for molecular analysis based on the presence of longitudinally sectioned crypts in the paraffin blocks that were available. The superficially located dysplastic cells and the underlying normal-appearing epithelial cells from the same crypts were microdissected under an inverted microscope. DNA was purified from the microdissected tissues by using a Qiaquick PCR purification kit (catalog no. 28104, Qiagen, Chatsworth, CA).

Immunoperoxidase Staining. Five-micrometer-thick sections obtained from formalin-fixed, paraffin-embedded tissue blocks were stained with a monoclonal Ki-67 antibody (AMAC, Westbrook, ME) or an anti-β-catenin antibody (Transduction Laboratories, Lexington, KY). The reactions were developed with avidin-biotin peroxidase and the reaction products detected after incubation with 3,3′-diaminobenzidine chromagen as described (10). The sections were counterstained with 0.1% hematoxylin (Sigma), dehydrated, and mounted. Immunoperoxidase staining was performed with the automated Bio Tek-1000 immunostainer system (Bio-Tek Solutions, Santa Barbara, CA).

Loss of Heterozygosity (LOH) Analysis. Four single-nucleotide polymorphic markers within the adenomatous polyposis coli (*APC*) gene were used to assess LOH (11, 12). Forward and reverse primers were designed for each single-nucleotide polymorphism (SNP), allowing the amplification of ≈100-bp PCR products. Digital PCR was performed as described (13, 14), by using primers and molecular beacons previously described (12). In brief, DNA was diluted and distributed to the wells of a 384-well plate (Robbins, Sunnyvale, CA) at <1 genomic equivalent per

Abbreviations: APC, adenomatous polyposis coli; LOH, loss of heterozygosity; SNP, single-nucleotide polymorphism.

§To whom reprint requests should be addressed. E-mail: vogelbe@welch.jhu.edu.

The publication costs of this article were defrayed in part by page charge payment. This article must therefore be hereby marked "*advertisement*" in accordance with 18 U.S.C. §1734 solely to indicate this fact.

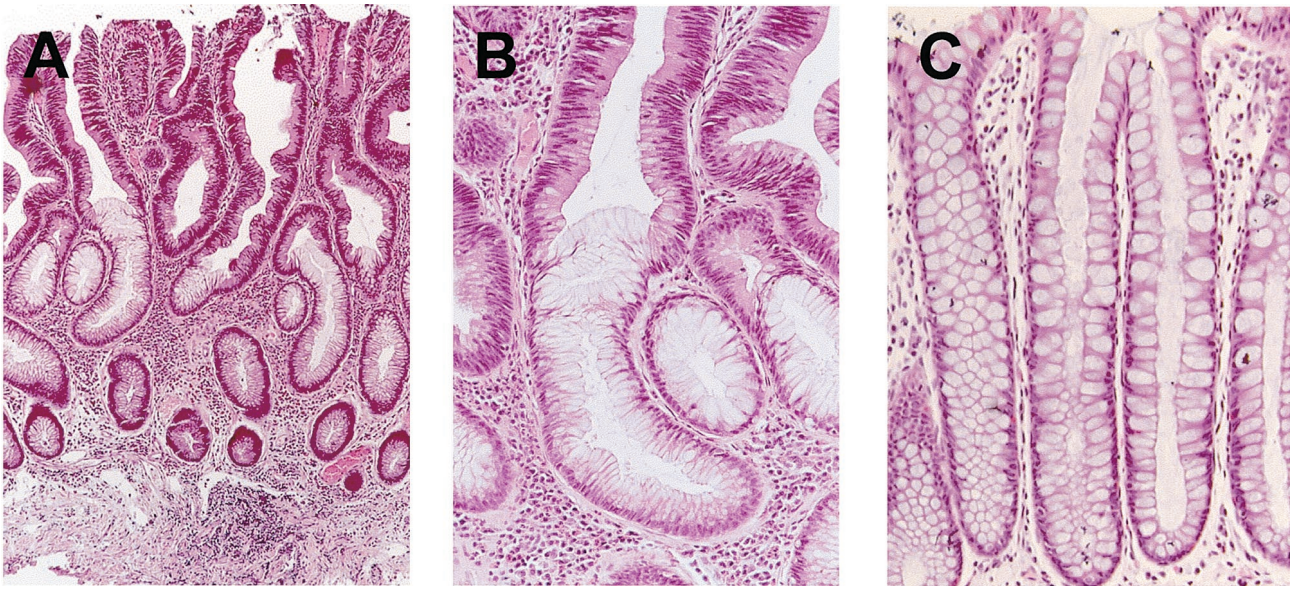

Fig. 1. (*A*) Hematoxylin and eosin stained section of a typical small adenomatous polyp. Dysplastic epithelium is located superficially in the crypts and is contiguous with the underlying histologically normal epithelium at the base. (*B*) Note the abrupt transition between dysplastic and normal-appearing epithelial cells at the mid-point of this crypt. (*C*) Adjacent normal colonic mucosae for comparison.

well. PCR was performed with a touch-down protocol: 94°C (1 m); four cycles of 94°C (15 s), 64°C (15 s), 70°C (15 s); four cycles of 94°C (15 s), 61°C (15 s), 70°C (15 s); four cycles of 94°C (15 s), 58°C (15 s), 70°C (15 s); and 45 cycles of 94°C for (15 s), 55°C (15 s), 70°C (15 s). After the PCR, a pair of molecular beacons (15, 16) was added to the final PCR product along with an internal primer that allowed the generation of single-stranded DNA complementary to the molecular beacons. For this asymmetric PCR step, the following conditions were used: 15 cycles of 94°C (15 s), 55°C (15 s), 70°C (15 s); and one cycle of 94°C (1 m), 60°C (5 m). The fluorescence intensity in each well was then measured with a Galaxy FLUOstar fluorometer (BMG Lab Technologies, Durham, NC), and the number of maternal and paternal alleles present in each sample was directly determined from the fluorescence measurements. A sequential probability ratio test was used to determine whether a specific sample exhibited LOH (14).

Nucleotide Sequence Analysis. A segment of the *APC* gene (codons 1,178–1,538) encompassing the mutation cluster region, i.e., codons 1,286–1,513 (17) was amplified in three overlapping segments. PCR amplification was performed on DNA prepared from microdissected specimens. DNA sequencing was performed on PCR products purified by using the Qiaquick PCR purification kit. The primer sets used for amplification were: segment 1: forward 5′-AGTGAAGAAAGCGGCCGCACGTCATGTGGATCAG-CCTATTG-3′ and reverse 5′-AGGCTTTCTCTCGAGGGATT-TGGTTCTAGGGTGCTGTGAC-3′; segment 2: forward 5′-AGTGAAGAAAGCGGCCGCAATACAGACTTATTGT-GTAGAAGATACTCC-3′ and reverse 5′-AGGCTTTCTCTC-GAGCGAACGACTCTCAAAACTATCAAG-3′; and segment 3: forward 5′-AGTGAAGAAAGCGGCCGCCCCACTCAT-GTTTAGCAGATGTAC-3′ and reverse 5′-AGGCTTTCTCTC-GAGAGGCTGCTCTGATTCTGTTTC-3′. The forward primers were used for sequencing, performed by using Sequitherm (Amersham Pharmacia) and [α-^{33}P]-labeled dideoxynucleotide triphosphates. Sequencing ladders were separated through electrophoresis in 4.5% denaturing acrylamide gels (Genomyx, Foster City, CA) and subjected to autoradiography.

Results

Microscopic examination of hematoxylin and eosin stained sections showed that dysplastic epithelium was uniformly present in the superficial (top) regions of the small adenomas studied. In each of the 35 cases analyzed, the dysplasia was confined to the orifice or luminal (top) regions of the crypts, whereas the basal regions of the crypts were morphologically normal (Fig. 1*A*). When an entire longitudinal crypt profile was visible in the plane of section, an abrupt transition between dysplastic and normal epithelium was always observed (Fig. 1*B*). This morphological feature was not evident in the adjacent normal mucosae (Fig. 1*C*).

To confirm that the dysplastic compartment at the top of the crypts represented abnormally proliferating cells, we stained the sections with Ki-67, an antibody that reacts with antigens in the nuclei of replicating but not quiescent cells (18). As shown in Fig. 2 *A* and *B*, the dysplastic compartment at the top of the crypts stained intensely with this antibody, in a pattern similar to what has been observed previously in larger adenomas and carcinomas (19–21). In contrast, the bottoms of the crypts, containing morphologically normal cells, exhibited a different pattern of staining. In particular, nuclei in the top one-half of the morphologically normal portion of the crypts were not stained with Ki-67, whereas nuclei in the bottom one-half of the morphologically normal portion were labeled. This recapitulated the pattern observed in completely normal crypts from regions of the colon far removed from any adenoma (Fig. 2*C*).

To gain insights into the mechanisms underlying these morphological and biochemical changes, we analyzed components of the *APC* pathway. It has been shown that mutations in *APC* or β-catenin initiate the vast majority of colorectal neoplasms. APC binds to β-catenin, stimulating β-catenin degradation and thereby inhibiting transcriptional activation of β-catenin/Tcf4 transcription complexes (22, 24). One way of evaluating the *APC* pathway is through immunohistochemical staining. When small adenomas were stained with the β-catenin antibody, the top portions of the crypts were intensely stained, with β-catenin present in the nucleus as well as in the cytoplasm and cell membranes (Fig. 3 *A* and *B*). The fraction of dysplastic cells exhibiting nuclear β-catenin staining varied from 65–85%. This

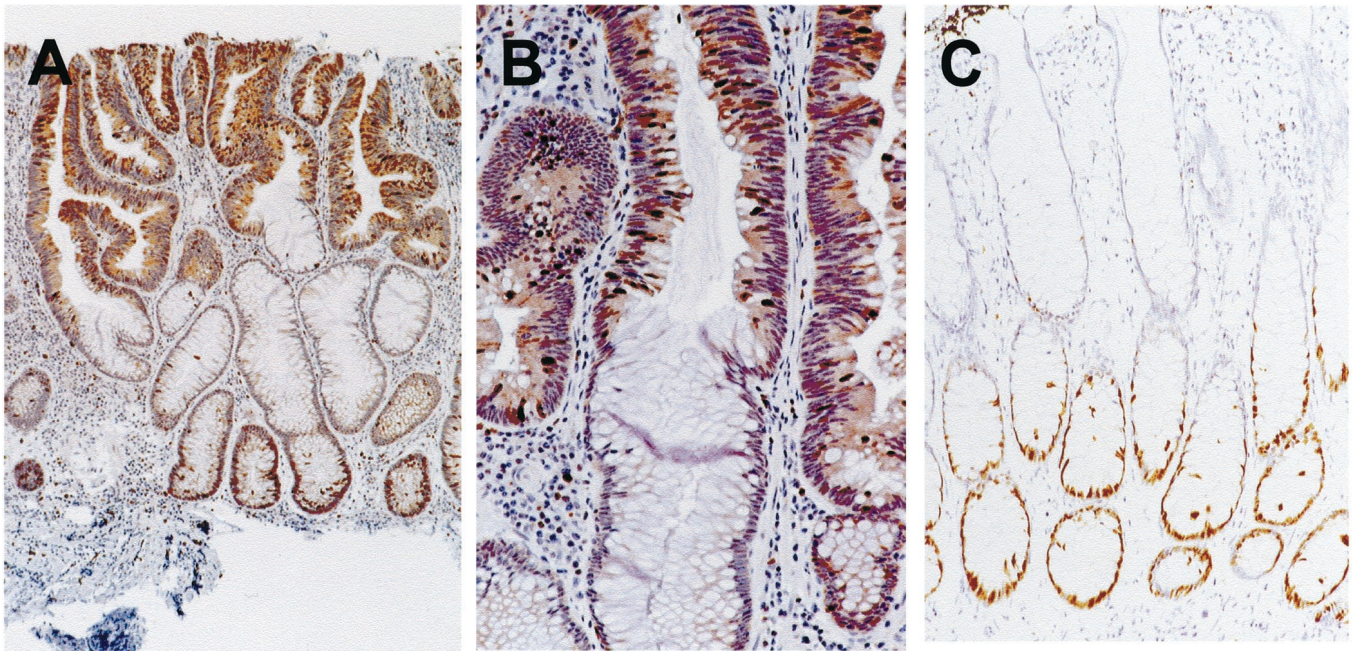

Fig. 2. Proliferative activity assessed with the Ki-67 antibody. Ki-67 immunoreactivity is broadly distributed throughout the dysplastic epithelium at the top of the crypts (*A* and *B*). Within the normal-appearing epithelium at the bottom of the crypts, only the basal and surrounding cell layers are labeled (*A* and *B*), similar to the pattern observed in normal colonic epithelium unassociated with neoplasia (*C*).

staining was similar to that previously observed in larger adenomas and carcinomas (23). In contrast, the bottoms of the crypts, containing morphologically normal cells, stained less intensely, with the staining largely confined to the cell membranes (Fig. 3 *A* and *B*). In non-neoplastic colonic epithelial cells, most β-catenin is bound to E-cadherin at the cell membrane, consistent with the observed pattern (Fig. 3*C*).

Although these β-catenin staining patterns were suggestive of *APC* pathway dysfunction, it was conceivable that they reflected epigenetic or reactive processes not indicative of genuine mutations in *APC*. To evaluate the *APC* gene within these lesions, we selected 10 small adenomas in which the sectioning plane allowed visualization of entire crypts, from the base to the orifice. An abrupt transition from adenomatous epithelium at the top to normal-appearing epithelium at the bottom was present in at least one crypt in each of these adenomas (example in Fig. 1). Careful microdissection was then used to isolate the dysplastic cells at the top of these crypts from the normal-appearing epithelium at the base.

In most large colorectal tumors, both alleles of *APC* are inactivated. In approximately one-half of these cases, one allele contains an intragenic stop codon whereas the other allele is deleted (loss of heterozygosity, ref. 24). To search for evidence of LOH at the *APC* locus, we used a recently described technique

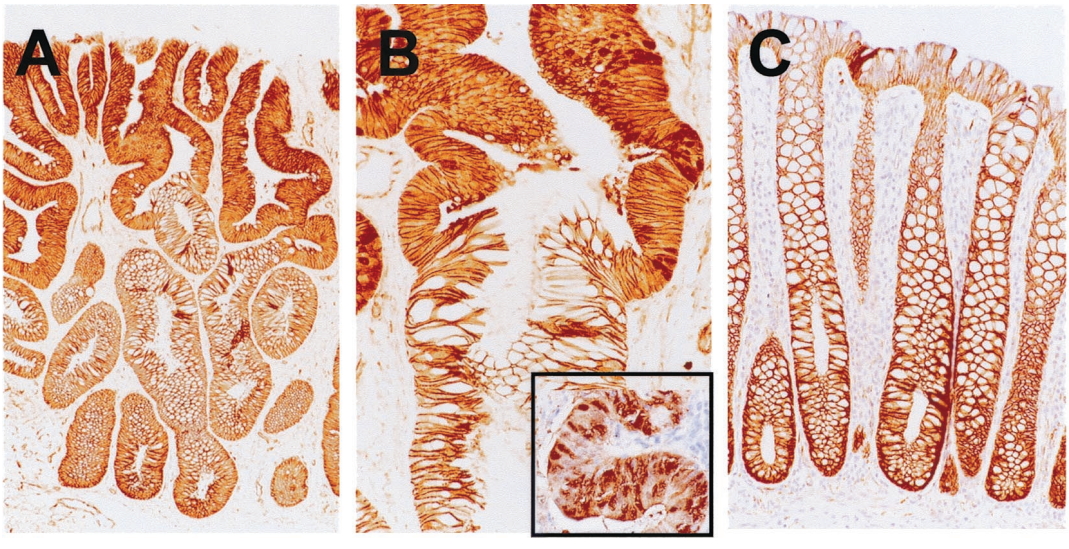

Fig. 3. β-Catenin expression in small adenomas. β-catenin is highly expressed and distributed throughout the dysplastic epithelium at the top of the crypts, where it is found in the nucleus as well as in the cytoplasm and plasma membrane (*A* and *B*). In contrast, staining is less intense in the normal-appearing epithelium at the bottom of the crypts, and staining is confined to the membranes (*A* and *B*). The staining pattern at the bottom of the adenomatous crypts is similar to that observed in normal colonic epithelium unassociated with neoplasia (*C*).

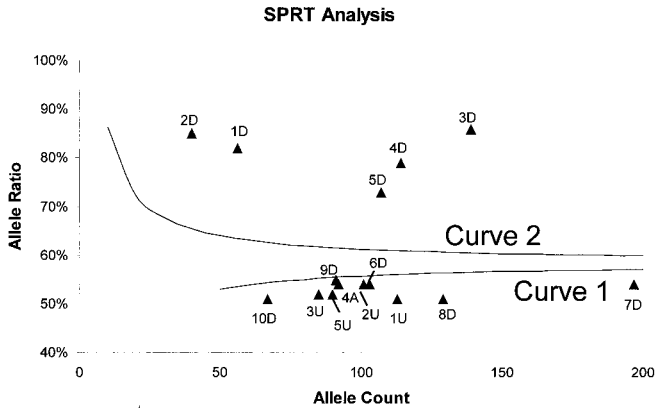

Fig. 4. Sequential probability ratio test analysis of LOH. Digital SNP analysis by using polymorphic markers within the *APC* gene was performed on the microdissected components of the adenomas. The resultant microdissected fractions consisted of dysplastic cells (D) from the tops of the crypts and underlying normal epithelium (U) from the same crypts. The *x* axis represents the total number of alleles counted, whereas the *y* axis represents the observed proportion of the two alleles. Samples whose observed allelic proportions was above curve 2 were interpreted to have undergone LOH, whereas samples whose observed allelic proportion was below curve 1 were interpreted as being in allelic balance. ▲, The allelic proportion of an individual DNA sample from the indicated crypt component, with the numbers corresponding to the adenomas listed in Table 1.

called digital SNP analysis. In this method, alleles within a DNA preparation are directly counted, one by one, and statistically analyzed (12, 14). Digital SNP thereby facilitates confident assessment of allelic status even when a proportion of the DNA in the analyzed samples is derived from non-neoplastic cells.

By using SNPs within the *APC* gene, we found that five of the 10 samples in our cohort had undergone LOH in their adenomatous, top portions. The data in Fig. 4, representing sequential probability ratio tests, show the observed allelic proportions together with curves depicting probabilities of allelic loss (curve 2) or allelic retention (curve 1) (25). Points above curve 2 represent samples in which there is a significant likelihood of allelic loss. The allelic proportions in the DNA isolated from the tops of the crypts ranged from 70–90%, perfectly consistent with estimates of the relative concentrations of neoplastic to non-neoplastic cells within the microdissected specimens. Of importance, the underlying histologically normal epithelial cells from these five lesions did not lose heterozygosity for these markers (Fig. 4).

We next determined whether the residual alleles of these dysplastic cells harbored inactivating mutations of *APC*. In light of the limiting amounts of DNA recovered from individual crypts within these adenomas, we could not evaluate the entire *APC* gene. We instead focused on the mutation cluster region of *APC* gene encompassing codons from 1178 to 1538, as previous studies have shown that >50% of colorectal cancers have truncating mutations within this region (17, 26). Direct sequencing of PCR products derived from cells from the tops of the crypts were used to search for such mutations. We were able to obtain sufficient DNA for analysis in four of the five lesions exhibiting LOH. In each of these four lesions, a truncating *APC* mutation was identified. Two of the mutations were due to nucleotide substitutions resulting in nonsense mutations whereas two were due to small deletions (Table 1). In each case, the mutant sequence was more intense than the wild-type sequence, consistent with a LOH event (examples in Fig. 5). The underlying histologically normal epithelial cells underlying the dysplastic cells contained only the wild-type *APC* sequence (Fig. 5).

Table 1. Summary of LOH and mutations of *APC* in adenomas

Specimen no.	Location	In APC	Mutation
1	Superficial adenomatous	LOH	1356 Ser → Stop
	Underlying ''normal''	R	wt
2	Superficial adenomatous	LOH	ND
	Underlying ''normal''	R	ND
3	Superficial adenomatous	LOH	FS (8-bp del at 1487)
	Underlying ''normal''	R	wt
4	Superficial adenomatous	LOH	FS (5-bp del at 1309)
	Underlying ''normal''	R	wt
5	Superficial adenomatous	LOH	1378 Gln → Stop
	Underlying ''normal''	R	wt
6	Superficial adenomatous	R	wt
	Underlying ''normal''	R	ND
7	Superficial adenomatous	R	1450 Arg → Stop
	Underlying ''normal''	R	wt
8	Superficial adenomatous	R	1367 Gln → Stop
	Underlying ''normal''	R	wt
9	Superficial adenomatous	R	FS (2-bp del at 1399)
	Underlying ''normal''	R	ND
10	Superficial adenomatous	R	wt
	Underlying ''normal''	R	ND

R, retained both alleles; wt, wild type; ND, not done (insufficient DNA); FS, frame shift; del, deletion of nucleotides.

The sequence of the *APC* mutation cluster region was also determined in the five tumors without LOH. Three of these cases contained truncating mutations, two due to nucleotide substitutions resulting in stop codons and one due to a 2-bp deletion (Table 1). In these cases, the ratio of mutant to mutation cluster region signals in the sequencing ladder was ≈1.0, consistent with the absence of an LOH event (data not shown). As in the cases with LOH, the mutations were confined to the dysplastic epithelium, and the morphologically normal epithelial cells at the bottoms of the crypts contained only the wild-type sequence (Table 1).

Discussion

The results described above demonstrate that small adenomas are usually composed of crypts with characteristic histologic, biochemical, and genetic features. The bases of the crypts consist of normal epithelial cells identical in all respects to those found

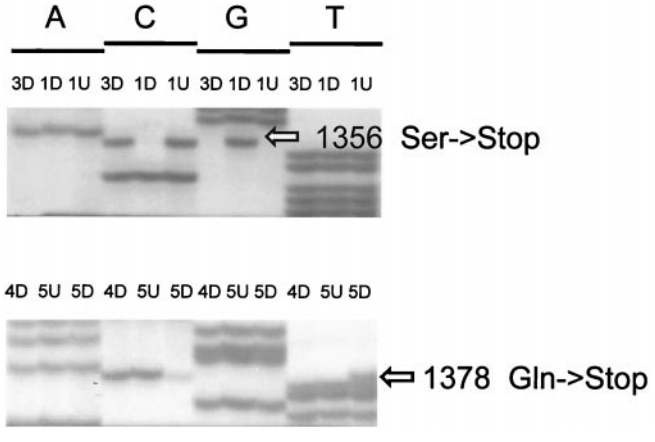

Fig. 5. Dysplastic epithelial cells harbor *APC* mutations. Examples of DNA sequencing gels of PCR products derived from microdissected components of the adenomas are shown. The microdissected fractions consisted of dysplastic cells (D) from the tops of the crypts and underlying normal epithelium (U) from the same crypts. The numbers refer to the adenomas listed in Table 1.

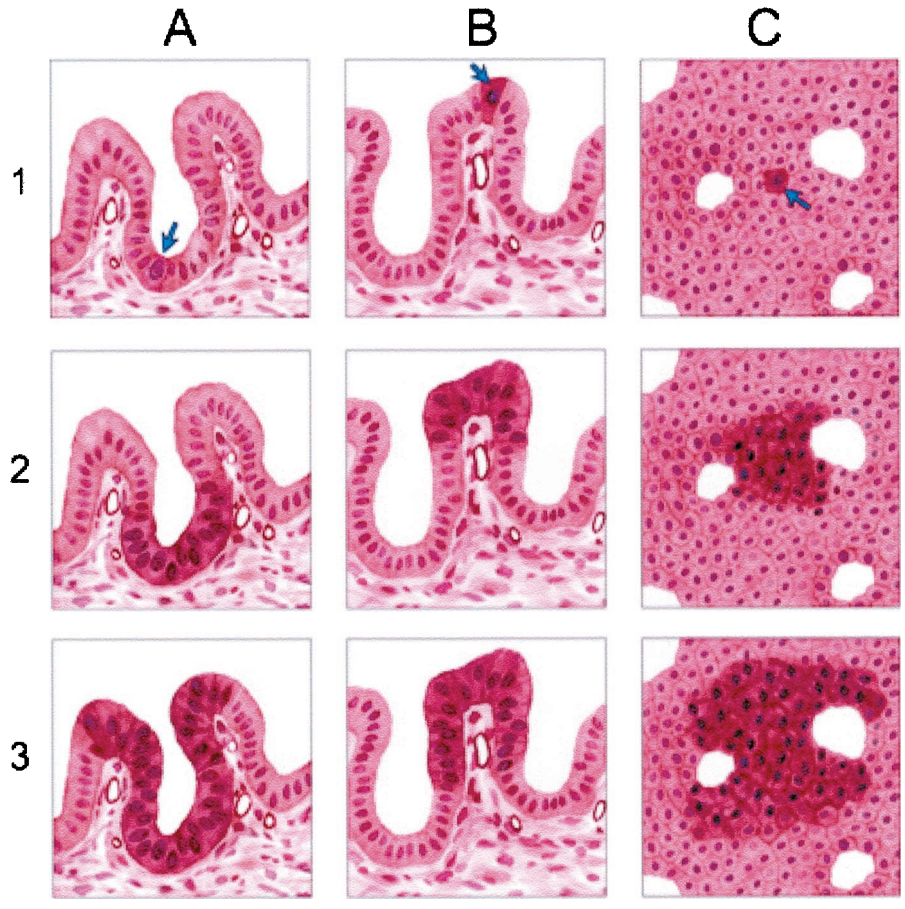

Fig. 6. Models of morphogenesis of sporadic adenomatous polyps. (*A*) Transformation of a single epithelial cell occurs at the base of the crypt (arrow) by virtue of *APC* inactivation. The transformed cell proliferates and passively migrates upward as a result of routine epithelial turnover. Once the transformed cells reach the superficial portion of the mucosae, they continue to proliferate and migrate and begin to populate the superficial mucosae of the adjacent crypts. The adenomatous epithelium thereby confronts the normal epithelium of the adjacent crypts, pushing the latter downward and gradually replacing it from top-to-bottom. (*B*) Similar to *A* except that the initial transformation event occurs in an epithelial cell in the intercryptal zone lying between crypt orifices (arrow). (*C*) *En face* view of surface, indicating spread of intercryptal dysplastic epithelial cell to adjacent crypts.

at the bases of crypts in normal colonic mucosae. However, this normal epithelial layer is contiguous with dysplastic epithelium that forms the top portion of the crypts and extends toward the orifice. In addition to the morphologic abnormalities, the dysplastic epithelium at the tops of the crypts displays a markedly abnormal pattern of proliferation when stained with Ki-67, identical to that observed in advanced neoplasms. Moreover, the superficial dysplastic epithelium generally contains genetic alterations at the *APC* locus associated with functional changes in β-catenin expression and localization.

It is worth emphasizing that the patterns summarized above did not represent an occasional occurrence in small adenomas; these patterns were virtually always present, in nearly every crypt of every small adenoma studied. It is highly unlikely that the inverted morphogenesis of small adenomas is an artifact due to tangential sectioning because the crypts with dysplastic and normal-appearing epithelium were entirely visible in suitably oriented sections. Furthermore, in our series of 35 small adenomas, there was not one example wherein all of the crypts were composed of uniformly dysplastic epithelium throughout their length, nor were any lesions observed in which the dysplastic epithelium was at the base of the crypts with normal overlying epithelium. Although our genetic and functional analyses are entirely novel, our morphological observations and assessment of proliferation status are consistent with a large number of observations made by other investigators over many years (3–7).

How can these data be reconciled with the conventional view that adenomas develop from stem cells located at the bases of normal crypts (reviewed in ref. 2)? From the data presented here, it is clear that the dysplastic process proceeds from the top-down rather than from the bottom-up. We envision two possible explanations for this top-down morphogenesis. First, the precursors of the dysplastic cells may actually reside in the intercryptal zones at the surface of the mucosae rather than at the base of the crypts. These dysplastic cells migrate laterally (Fig. 6*C*) and downward (Fig. 6*B*), pushing the normal epithelium in adjacent crypts toward the bottom of the mucosal layer. The sites where dysplastic epithelium from the top meets normal epithelium would be predicted to result in an abrupt transition, as seen in Figs. 1–3. Although this model challenges the conventional view of stem cells, it is supported by experimental studies demonstrating that the intercryptal zone, rather than the base of crypts, appears to be the repository for stem cells that repopulate the colon after epithelial denudation (S.B.-S., unpublished observations).

A second explanation for the top-down model is that the neoplastic cells originate in stem cells at the bases of crypts, but that the transformed cells initially migrate up the crypt and thereafter become part of the superficial mucosae as in the first explanation (Fig. 6*A*). We cannot rule out the possibility that each adenoma we studied originated from the base of a single crypt which was not visible in our sections, and that all other

crypts in the adenoma represent the result of spreading once the original transformed cell from the crypt base reached the surface. The histogenesis of human colorectal adenomas is distinct from that in mice with heritable mutations of *APC*. In mice, the incipient adenomas are formed by outpocketing pouches near the bases of the crypts that protrude into the lacteal side of neighboring crypts (27). Such outpocketing and invasion would not be predicted to result in the crypt morphogenesis patterns characteristic of small human adenomas (Fig. 1), and the morphological pattern depicted in Fig. 1 has never been observed in mice. Whether these differences reflect the different species involved, or the fact that most adenomas in mice occur in the small rather than the large intestine, is not known. Another difference between mouse and human adenomas is that the former are almost always covered on their surface by a single layer of normal epithelium (27), whereas such carpeting is never observed in human tumors.

Maskens *et al.* (5) have studied the morphologic development of neoplasia in familial adenomatous polyposis patients, who have heritable mutations in *APC*. Because of the large numbers of lesions that could be studied in these patients, Maskens *et al.* (5) were able to evaluate incipient adenomas at very early stages, more primitive than those studied here. These very small lesions appeared to develop through a top-down process such as depicted in Fig. 6. As the small familial adenomatous polyposis adenomas progressed to larger ones (>1 cm), the normal epithelial cells at the base of the crypts were completely replaced by dysplastic epithelium. Hence, the development of adenomas in this familial form of human cancer is quite similar to that in sporadic forms, presumably because both are initiated by the inactivation of both *APC* alleles in the same precursor cells.

Appreciation of the basic features of early adenoma formation should lead to a greater understanding of the initiation of colorectal neoplasia. Moreover, these data have significant implications for research on intestinal stem cells and their migratory capacity.

We thank Dr. Elizabeth Montgomery of the Department of Pathology at Johns Hopkins Hospital for the critical review of this manuscript and the Johns Hopkins Oncology Center Cell Imaging Core Facility for assistance with photography. Under a licensing agreement between the Johns Hopkins University and EXACT Laboratories, digital PCR technology was licensed to EXACT, and B.V. and K.W.K. are entitled to a share of royalties received by the University from sales of the licensed technology. The terms of these arrangements are being managed by the University in accordance with its conflict of interest policies. This work was supported by the Clayton Fund, the V Foundation, and National Institutes of Health Grants CA43460, CA57345, and CA62924.

1. Garcia, S. B., Park, H. S., Novelli, M. & Wright, N. A. (1999) *J. Pathol.* **187,** 61–81.
2. Bach, S. P., Renehan, A. G. & Potten, C. S. (2000) *Carcinogenesis* **21,** 469–476.
3. Cole, J. W. & McKalen, A. (1963) *Cancer (Philadelphia)* **16,** 998–1002.
4. Lipkin, M. (1974) *Cancer (Philadelphia)* **34** Suppl. 878–888.
5. Maskens, A. P. (1979) *Gastroenterology* **77,** 1245–1251.
6. Wiebecke, B., Brandts, A. & Eder, M. (1974) *Virchows Arch. A Pathol. Anat. Histol.* **364,** 35–49.
7. Nakamura, S. & Kino, I. (1984) *J. Natl. Cancer Inst.* **73,** 41–49.
8. Polyak, K., Hamilton, S. R., Vogelstein, B. & Kinzler, K. W. (1996) *Am. J. Pathol.* **149,** 381–387.
9. Lane, N. & Lev, R. (1963) *Cancer (Philadelphia)* **16,** 751–764.
10. Shih, I. M., Seidman, J. D. & Kurman, R. J. (1999) *Hum. Pathol.* **30,** 687–694.
11. Powell, S. M., Zilz, N., Beazer-Barclay, Y., Bryan, T. M., Hamilton, S. R., Thibodeau, S. N., Vogelstein, B. & Kinzler, K. W. (1992) *Nature (London)* **359,** 235–237.
12. Shih, I.-M., Zhou, W., Goodman, S. N., Lengauer, C., Kinzler, K. W. & Vogelstein, B. (2001) *Cancer Res.* **61,** 818–822.
13. Vogelstein, B. & Kinzler, K. W. (1999) *Proc. Natl. Acad. Sci. USA* **96,** 9236–9241.
14. Zhou, W., Galizia, G., Goodman, S., Romans, K., Lieto, E., Kinzler, K. W., Vogelstein, B., Choti, M. & Montgomery, E. (2001) *Nat. Biotechnol.*, **19,** 78–81.
15. Tyagi, S. & Kramer, F. R. (1996) *Nat. Biotechnol.* **14,** 303–308.
16. Tyagi, S., Bratu, D. P. & Kramer, F. R. (1998) *Nat. Biotechnol.* **16,** 49–53.
17. Miyoshi, Y., Nagase, H., Ando, H., Horii, A., Ichii, S., Nakatsuru, S., Aoki, T., Miki, Y., Mori, T. & Nakamura, Y. (1992) *Hum. Mol. Genet.* **1,** 229–233.
18. Gerdes, J., Lemke, H., Baisch, H., Wacker, H. H., Schwab, U. & Stein, H. (1984) *J. Immunol.* **133,** 1710–1715.
19. Sahin, A. A., Ro, J. Y., Brown, R. W., Ordonez, N. G., Cleary, K. R., el-Naggar, A. K., Wilson, P. & Ayala, A. G. (1994) *Mod. Pathol.* **7,** 17–22.
20. Kikuchi, Y., Dinjens, W. N. & Bosman, F. T. (1997) *Virchows. Arch.* **431,** 111–117.
21. Sakuma, K., Fujimori, T., Hirabayashi, K. & Terano, A. (1999) *J. Gastroenterology* **34,** 189–194.
22. Polakis, P. (2000) *Genes Dev.* **14,** 1837–1851.
23. Iwamoto, M., Ahnen, D. J., Franklin, W. A. & Maltzman, T. H. (2000) *Carcinogenesis* **21,** 1935–1940.
24. Kinzler, K. W. & Vogelstein, B. (1996) *Cell* **87,** 159–170.
25. Royall, R. (1997) *Statistical Evidence: A Likelihood Primer* (Chapman & Hall, London).
26. Yashima, K., Nakamori, S., Murakami, Y., Yamaguchi, A., Hayashi, K., Ishikawa, O., Konishi, Y. & Sekiya, T. (1994) *Int. J. Cancer* **59,** 43–47.
27. Oshima, H., Oshima, M., Kobayashi, M., Tsutsumi, M. & Taketo, M. M. (1997) *Cancer Res.* **57,** 1644–1649.